ORIGINAL PAPER

Cu–Fe Incorporated Graphene-Oxide Nanocomposite as Highly Efficient Catalyst in the Degradation of Dichlorodiphenyltrichloroethane (DDT) from Aqueous Solution

Giang H. Le[1] · Tuan T. Nguyen[2] · Manh B. Nguyen[1] · Trang T. T. Quan[1] · Trinh Duy Nguyen[3] · Andras Sapi[4] · Imre Szenti[4] · Suresh Mutyala[4] · Akos Kukovecz[4] · Zoltan Konya[4] · Tuan A. Vu[1]

Abstract

Fe/graphene oxide and Cu–Fe/graphene oxide nanocomposite were synthesized by the atomic implantation method to study the photocatalytic degradation of dichlorodiphenyltrichloroethane (DDT). The synthesized nanocomposites were characterized by the XRD, N_2 isotherms, SEM with EDX, TEM and XPS analysis. Characterization results have reported that oxides of Cu and Fe were uniformly distributed on graphene oxide and exited in the form of Cu^+ and Fe^{2+} ions in Cu–Fe/graphene oxide nanocomposite. The high photocatalytic DDT removal efficiency 99.7% was obtained for Cu–Fe/graphene oxide under the optimal condition of 0.2 g/L catalyst, 15 mg/L H_2O_2 and pH 5. It was attributed to the reduction of Fe^{3+} to Fe^{2+} by Cu^+ ions and –OH radicals formation. However, it was dropped to 90.4% in the recycling study by leaching of iron and without a change in phase structure and morphology.

Graphic Abstract
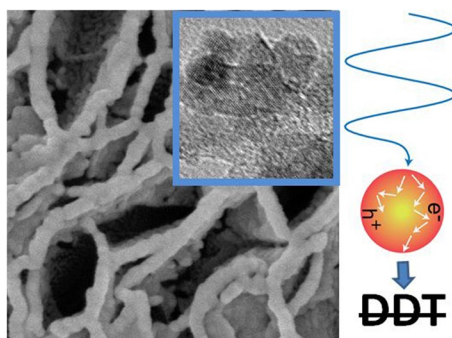
✉ Andras Sapi
sapia@chem.u-szeged.hu

1 Institute of Chemistry, Vietnam Academy of Science and Technology, 18 Hoang Quoc Viet Street, Cau Giay, Hanoi, Vietnam

2 Graduate University of Science and Technology, Vietnam Academy of Science and Technology, 18 Hoang Quoc Viet Street, Cau Giay, Hanoi, Vietnam

3 Center of Excellence for Green Energy and Environmental Nanomaterials (CE@GrEEN), Nguyen Tat Thanh University, Nguyen Tat Thanh, District 4, Ho Chi Minh City 300A, Vietnam

4 Department of Applied and Environmental Chemistry, Interdisciplinary Excellence Centre, Univesity of Szeged, H-6720, Rerrich Bela ter 1, Szeged, Hungary

1 Introduction

Dichlorodiphenyltrichloroethane (DDT), polychlorinated biphenyl (PCB), Dioxin and Furan are persistent organic pollutants that affect human health and the environment [1]. A few methods have been developed to eliminate/degrade these pollutants such as adsorption, biodegradation, and chemical degradation [2, 3]. Nano-structured zero-valent iron was claimed as a highly active site to degrade DDT in water and soil. Kang et al. have synthesized micro/nano-structured zero-valent iron (MNZVI) by ball-milling industrially reduced iron powder. Plate-like morphology of MNZVI exhibited high degradation performance compared to commercial zero-valent iron powder [4]. Yehia et al. have also synthesized nano-sized zero-valent iron (NZVI) by different methods. It has shown high degradation of DDT in water compared to soil [5]. Later, Tian et al. has synthesized bimetallic Ni/Fe nanoparticles to degrade DDT in aqueous solution. In this catalyst, Fe nanoparticles promoted Fenton reaction and Ni nanoparticles promoted dehydrochlorination [6].

The advanced oxidation process is one of the effective methods to degrade toxic pollutants. This refers to an oxidation process through the formation of hydroxyl radical which promoted the degradation of organic contaminants in water and subsequently it reacts with organic contaminants through a series of multiple steps to form non-toxic products like low molecular weight carboxylic acid, HCl, CO_2 and H_2O [7]. In the Fenton process, iron-catalyzed hydrogen peroxide (Fe^{2+}/H_2O_2) has been used for the removal of pollutants in water. It shows high degradation efficiency, simple operation and low toxicity [8]. However, it has some drawbacks such as lack of recovery of the catalyst, inefficiency in aqueous media (pH 5–9), production of a large amount of sludge and requires further treatment. In order to overcome these drawbacks, a heterogeneous Fenton process using iron-based catalysts such as Fe_2O_3, Fe_3O_4, FeOOH, Fe powder, Fe-MOF, Fe-Fe_3O_4 nanoparticles have been developed [9–13]. In this process, oxidation occurs at the solid–liquid interface where iron remains either in the solid phase and/or adsorbed ion.

Few research groups have synthesized composite materials such as Fe_3O_4/CeO_2 [12], Fe-g-C_3N_4/graphitized mesoporous carbon [14], graphene oxide–Fe_2O_3 [15], Cu-rGO [16], Fe_3O_4–CuO–graphene oxide [17], Fe–Fe_3O_4/graphene oxide [18], graphene oxide-amorphous $FePO_4$ [19] and graphene oxide/Fe-MOF [13] to degrade pollutants in aqueous solution. Among these, supporting materials like graphene and graphene oxide have great interest due to their unique structure, high specific surface area, chemical stability, conductivity and visible light adsorption ability [20, 21]. So, graphene oxide was considered

as a support to synthesize nanocomposite material. In this article, Fe/graphene oxide and Cu–Fe/graphene oxide nanocomposite were synthesized to study the degradation of DDT under light irradiation. The effect of catalyst concentration, pH and H_2O_2, intermediate products formed during the degradation of DDT and recyclability were studied.

2 Experimental

2.1 Chemicals

All analytical grade chemicals such as iron (II) chloride hexahydrate ($FeCl_3 \cdot 6H_2O$), copper (II) chloride tetrahydrate ($CuCl_2 \cdot 4H_2O$), graphite (C), dichlorodiphenyltrichloroethane ($C_{14}H_9Cl_5$), sulphuric acid (H_2SO_4), phosphoric acid (H_3PO_4), hydrochloric acid (HCl), hydrogen peroxide (30 wt% H_2O_2), and potassium permanganate ($KMnO_4$) were purchased from M/s. Sigma Aldrich Chemicals Pvt. Ltd., Vietnam. Ultra-high pure nitrogen gas cylinder was purchased from the local vendor, Vietnam.

2.2 Synthesis of Graphene Oxide

Graphene oxide was synthesized by the modified Hummer's method [22]. About, 1 g of graphite flakes were transferred into a mixture of 150 mL concentrated H_2SO_4 and H_3PO_4 (4:1, v/v (%)), stirred at room temperature for 1 h then 6 g of $KMnO_4$ was added slowly. The mixture was kept at room temperature for 3 days. It was turned dark brown from dark green. The oxidation reaction was quenched using 600 mL ice-cold water and 3 mL H_2O_2. The color of the solution was changed into bright yellow then it was centrifuged and washed with 1 M HCl to remove excess manganese salt. Finally, it was washed with distilled water until neutral pH obtained then dried at 100 °C overnight. The dried compound graphene oxide was labeled as GO.

2.3 Synthesis of Fe/GO and Cu–Fe/GO Nanocomposite

Fe/GO and Cu–Fe/GO nanocomposite were synthesized by the atomic implantation method using the equipment shown in Fig. 1. For the synthesis of Fe/GO, a desired quantity of iron (III) chloride hexahydrate and graphene oxide (Fe:GO = 20:80 wt%) were mixed and loaded at the center of the tubular furnace. It was heated at 500 °C for 30 min with a heating rate of 5 °C/min in a nitrogen atmosphere then cooled to room temperature slowly. Similarly, Cu–Fe/GO was prepared using the procedure the same as that of Fe/GO synthesis with precursors composition ratio (Cu:Fe:GO = 2:18:80 wt%).

Fig. 1 The schematic diagram for the synthesis of Fe/GO and Cu–Fe/GO nanocomposite
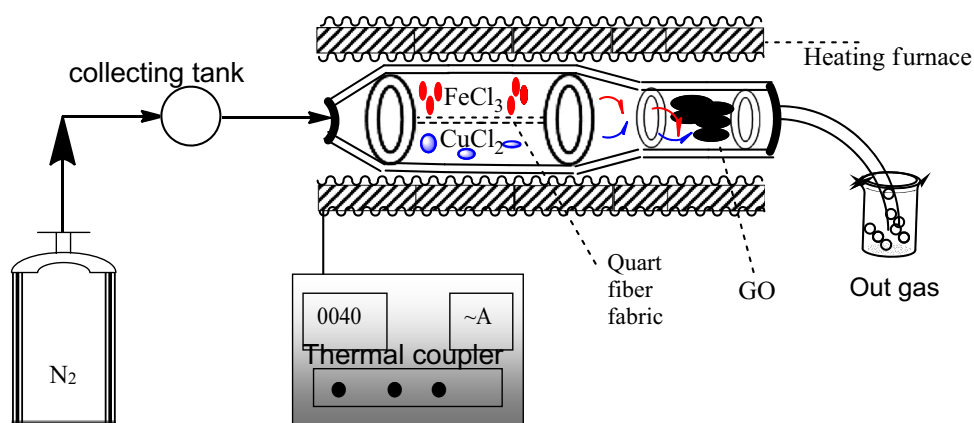
2.4 Characterization

X-ray diffractions were recorded using a D8 Advance X-ray diffractometer having Ni filtered Cu K_α radiation in the scan range from $2\theta = 5°$ to $70°$. Trista Plus II gas adsorption analyzer was used to measure adsorption–desorption isotherms at 77 K. Before the study of N_2 isotherms, 0.1 g of sample was degasified at 200 °C for 2 h under vacuum. The BET method was used to calculate the specific surface area and the t-plot method was used to calculate micropore volume. The total pore volume was calculated at a relative pressure of 0.99. FT-IR spectra were recorded using JACOS 4700 FT-IR spectrometer in the scan range from 4000 to 400 cm^{-1} with a resolution of 4 cm^{-1} using KBr. TEM image was obtained on a JEOL JEM 1400 transmission electron microscopy instrument operated at a voltage of 100 kV. Thermo Fisher K-alpha X-ray photoelectron spectrometer (ESCALAB MKII) was used to record the spectrum. SEM with Energy Dispersive X-ray spectroscopy (EDX) mapping was performed using a HITACHI S-4800.

2.5 Photocatalytic Degradation Experiment

Photocatalytic degradation of dichlorodiphenyltrichloroethane (DDT) in aqueous solution was studied using synthesized composite materials by irradiation of simulated sunlight UV-A 315–400 nm (4 lamps, power 15 W). The distance of the tested sample from the source of irradiated light was 20 cm and brightness was $2.03.10^4$ lx (M6M PRO Lux Meter LX 1010 BS-Taiwan). The experiment was performed in a Pyrex glass contacting 100 mL DDT solution at a concentration of 10 mg/L. The reaction parameters such as catalyst dosage 0.05–0.4 g/L, effect of pH 3–8 and concentration of H_2O_2 10–100 mg/L were also studied. Firstly, the reaction mixture was stirred in a dark condition to measure adsorption–desorption equilibrium on the surface of the catalyst. Secondly, it was exposed to sunlight with continuous stirring. The mixture was collected at regular intervals of time, centrifuged and analyzed using GC–MS Agilent

GC 7890A, MS 5975C spectrometer. The intermediate products were analyzed using LC–MS HRAM (Thermo Fisher) instrument with a column of Ultra aqueous C18.5 μm. The DDT degradation efficiency (%) was calculated using the following equation.

$$\text{Degradation efficiency}\% = \frac{C_0 - C_t}{C_0} \times 100$$

where C_0 is the initial concentration and C_t is the concentration at time t.

3 Results and Discussion

3.1 Structure, Chemical Composition, and Morphology

3.1.1 XRD and FT-IR Analysis

The crystalline structure and functional groups of synthesized composite materials were analyzed by XRD and FT-IR techniques. The XRD patterns of GO, Fe/GO and Cu–Fe/GO were shown in Fig. 2a. Pristine graphene oxide has shown a single diffraction peak at $2\theta = 10.6°$ with a reflection plane (001). The diffraction pattern of GO was matched with previously reported one [23]. In Fe/GO, the diffraction peaks of Fe_2O_3 were 24.1°, 33.1°, 36.5°, 40.8°, 49.4°, 54.1°, 57.5°, 62.3° and 64° having planes (012), (104), (110), (113), (024), (116), (018), (214) and (300) respectively (JCPDS card no. 39-1346) [24]. Moreover, Cu–Fe/GO has also shown diffraction peaks similar to Fe/GO. The copper oxide peaks have not appeared due to low particle size and/ or undetectable by the XRD [25]. In both Fe/GO and Cu–Fe/GO nanocomposite materials, the GO peak at $2\theta = 10.6°$ was absent which indicated that oxides of Fe and Cu were intercalated within graphene oxide layer [26]. Moreover, the crystalline GO was converted into amorphous GO during the synthesis of nanocomposite material.
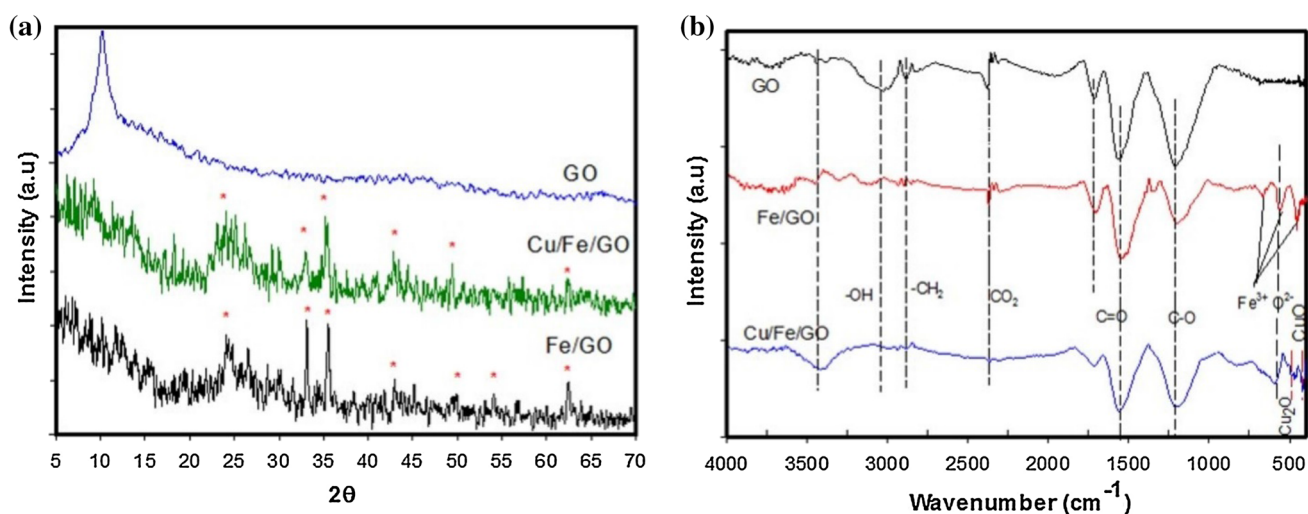
(a)

(b)

Fig. 2 **a** XRD patterns and **b** FT-IR spectra of GO, Fe/GO and Cu–Fe/GO

Figure 2b shows the FT-IR spectra of GO, Fe/GO and Cu–Fe/GO. The pristine graphene oxide has shown the vibrational bands at 3419 cm^{-1}, 2905 cm^{-1}, 2850 cm^{-1}, 2360 cm^{-1}, 1725 cm^{-1}, and 1230 cm^{-1} which correspond to stretching of O–H, C–H, O–C–O, C=O, C–O groups respectively [27]. For Fe/GO and Cu–Fe/GO nanocomposite materials, the major vibrational bands of graphene oxide were replicated. Along with this, a few new vibrational bands appeared at 630 cm^{-1}, 570 cm^{-1} and 480 cm^{-1} for Fe/GO which were related to Fe–O group of Fe_2O_3. Similarly, the bands at 506 cm^{-1} and 430 cm^{-1} were related to the Cu–O group of Cu_2O/CuO for Cu–Fe/GO nanocomposite [28–30].

3.1.2 XPS Analysis

The oxidation state of Fe and Cu in Cu–Fe/GO nanocomposite can be known by XPS analysis. Figure 3 shows the XPS spectra of Cu–Fe/GO. The survey spectrum has shown binding energies at 285 eV, 530 eV, 711 eV, and 934 eV which correspond to C1s, O1s, Fe2p and Cu2p (Fig. 3a). It indicated that these elements were present in synthesized nanocomposite material Cu–Fe/GO. By deconvolution of Fe2p peak obtained binding energies at 710 eV ($Fe2p_{3/2}$) and 724 eV ($Fe2p_{1/2}$). It reported that the existence of Fe_2O_3 [31]. Low-intensity peaks at 715 eV and 730 eV correspond to the presence of Fe(II)O in the synthesized material [32]. It is important to note that in the case of Fe/GO only the presence of Fe^{3+} is could be observed. Copper peak on deconvolution obtained binding energies at 931 eV and 943 eV and 951 eV which described the formation of Cu(II)O material [29]. The peak obtained at 931 eV indicated the presence of Cu_2O. The existence of both Cu^+, Cu^{2+}, and Fe^{2+} in Fe–Cu/GO indicated that the part of Fe^{3+} was reduced to Fe^{2+} by Cu^+. The deconvolution peaks of C1s were 284.4 eV, 285.6

eV, and 288.3 eV which described bonding of C–C, C–O, and O=C–O in graphene oxide sheets. The deconvolution peaks of O1s were 529.9 eV, 531.1 eV, and 533 eV which correspond to Fe–O, C=O and C–O respectively.

3.1.3 TEM and SEM with EDX Analysis

TEM and SEM with EDX mapping of Cu–Fe/GO were shown in Fig. 4. TEM image has reported that oxides of Cu and Fe were highly dispersed on graphene oxide and particle size was in the nano range (Fig. 4a). Porous network graphene oxide layers were appeared in the SEM image (Fig. 4b). EDX mapping of Cu and Fe has confirmed that CuO and Fe_2O_3 were uniformly dispersed by the atomic implantation method (Fig. 4c, d). The chemical composition of Fe/GO and Cu–Fe/GO was presented in Fig. 4e. The wt% of copper and iron obtained experimentally was near to theoretically loaded amount.

3.1.4 N_2 Adsorption–Desorption Isotherms

Figure 5 shows the N_2 adsorption–desorption isotherms and pore size distribution of GO and Cu–Fe/GO. The textural properties were presented in Table 1. The pristine graphene oxide has shown a hysteresis loop between the relative pressure $P/P_0 = 0.45$–1. According to the classification of porous materials, the isotherm pattern of GO is similar to type-IV with the H3 hysteresis loop which indicated that the presence of mesopores [33]. The BET surface area, total pore volume, and pore size of GO were 331 $m^2\ g^{-1}$, 1.719 $cm^3\ g^{-1}$ and 20.7 nm respectively. Cu–Fe/GO nanocomposite material has also shown an isotherm pattern similar to that of GO. But, the amount of N_2 adsorption was decreased. Hence, there was a change in the textural properties has been
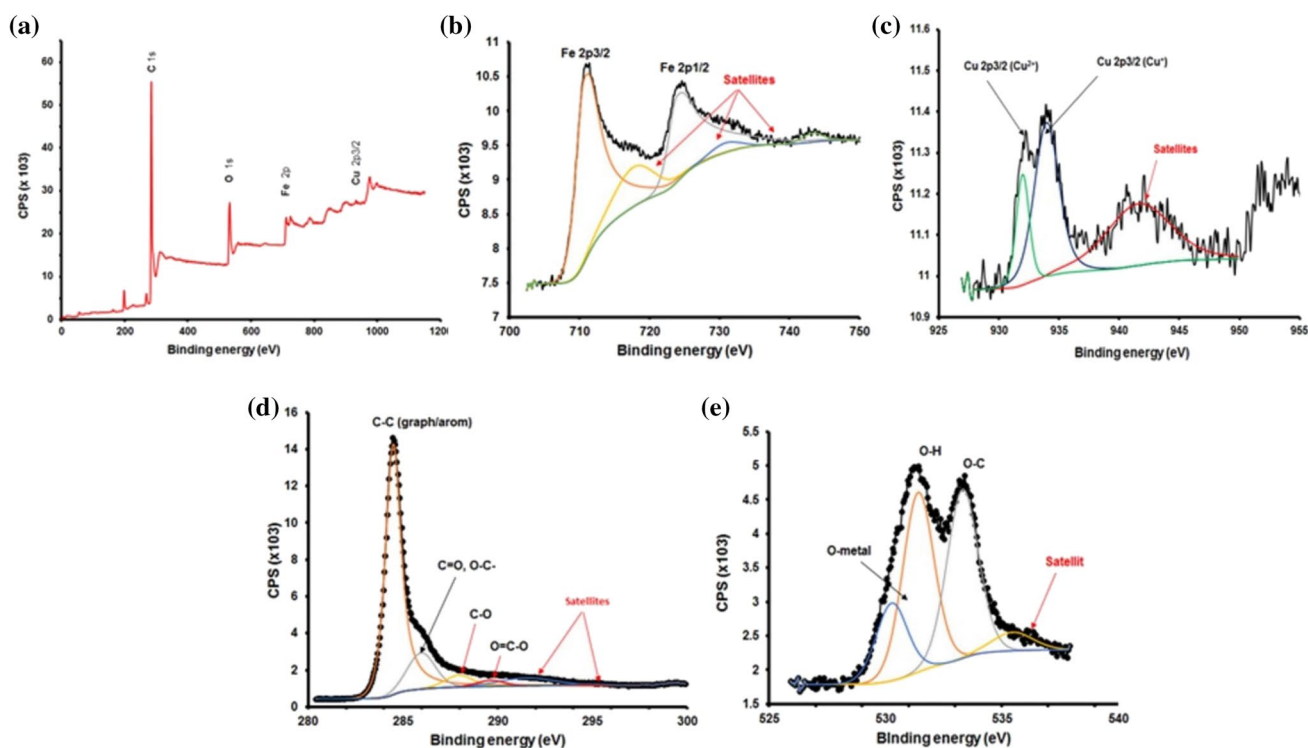
Fig. 3 XPS spectra of Cu–Fe/GO **a** survey, **b** Fe2p, **c** Cu2p, **d** C1s and **e** O1s

observed. The specific surface area, total pore volume and pore size of Cu–Fe/GO were decreased to 130 $m^2 g^{-1}$, 0.410 $cm^3 g^{-1}$ and 12.6 nm respectively. It was due to the blockage of pores by CuO and Fe_2O_3.

3.2 Photocatalytic Degradation of Dichlorodiphenyltrichloroethane

3.2.1 Parameters Influence on DDT Degradation

Effect of catalyst dosage The effect of Cu–Fe/GO dosage for the photocatalytic degradation of DDT was studied using 10 mg/L DDT solution, 15 mg/L H_2O_2, and pH 5 for 3 h. The DDT removal efficiency values were shown in Fig. 6. At the low dosage of catalyst 0.05 g/L, DDT removal efficiency was 53%. With an increase in catalyst dosage from 0.05 g/L to 0.2 g/L, the removal efficiency was increased and reached to 99.7%. Beyond 0.2 g/L of catalyst dosage, there was no change in degradation efficiency. Hence, the optimum amount of the catalyst for the degradation of DDT was 0.2 g/L for 10 mg/L of DDT solution. It was due to that 0.2 g/L of the catalyst has enough active adsorption sites to degrade the DDT solution. For high concentrated DDT solution, a high catalyst dosage might be needed [34].

Effect of pH The photocatalytic degradation of pollutant in the polluted water depends on the pH of the solution because pollutant has different pH values in aqueous solution [35]. Figure 7 shows the photocatalytic degradation of DDT at different pH of DDT solution using 0.2 g/L of Cu–Fe/GO, 15 mg/L H_2O_2 for 3 h. The DDT removal efficiency was 99.8% at pH 3 and 5. However, at higher pH > 5 the DDT removal efficiency was decreased and reached 91% (pH 8). The change in the photocatalytic activity of Cu–Fe/GO nanocomposite was due to the decomposition of H_2O_2. At pH > 5, H_2O_2 was decomposed into H_2O then active centers CuO and Fe_2O_3 were converted into the corresponding hydroxide [36, 37]. Hence, the photocatalytic activity of Cu–Fe/GO was decreased. At pH 3–5, hydroxy radicals were formed during the reaction which enhanced photocatalytic activity of Cu–Fe/GO to degrade DDT [38].

Effect of H_2O_2 dosage The effect of H_2O_2 concentration in photocatalytic degradation of DDT using Cu–Fe/GO was also studied. The conditions were 10 mg/L of DDT solution, 0.2 g/L of catalyst and pH 5, for 3 h (Fig. 8). With increase in concentration of H_2O_2 from 10 to 15 mg/L, DDT removal/degradation efficiency was increased from 85.6 to 99.2%. At a high dosage of H_2O_2 (30 mg/L, 60 mg/L, and 100 mg/L) removal efficiency was decreased. The change in DDT degradation efficiency was due to the formation of an optimal amount of hydroxy radicals in low concentration of H_2O_2 whereas at high concentration excess amount of H_2O_2 reduced hydroxy radicals (Eqs. 1 and 2) [34].

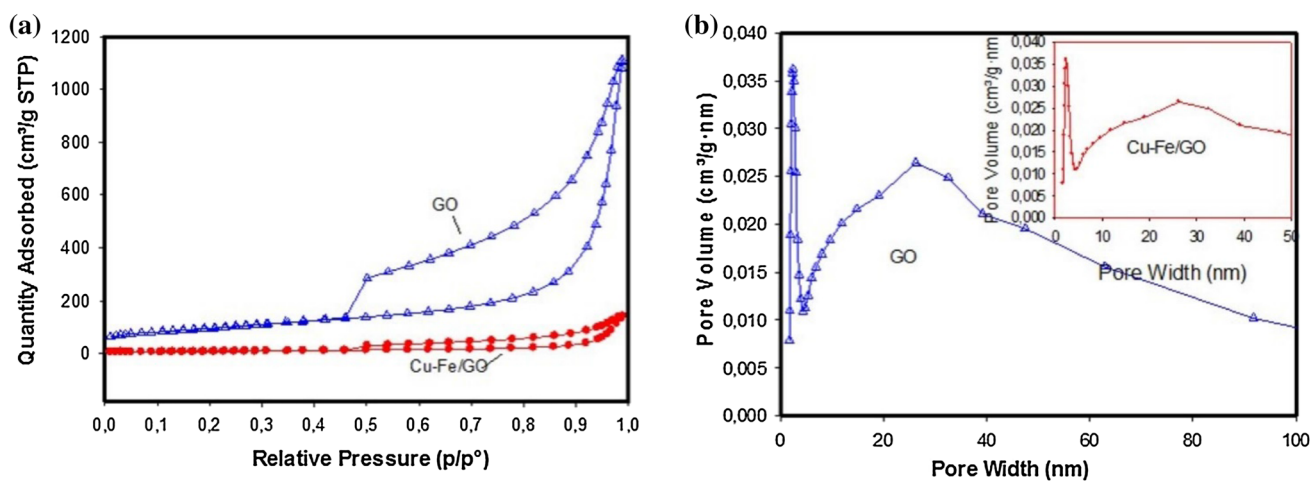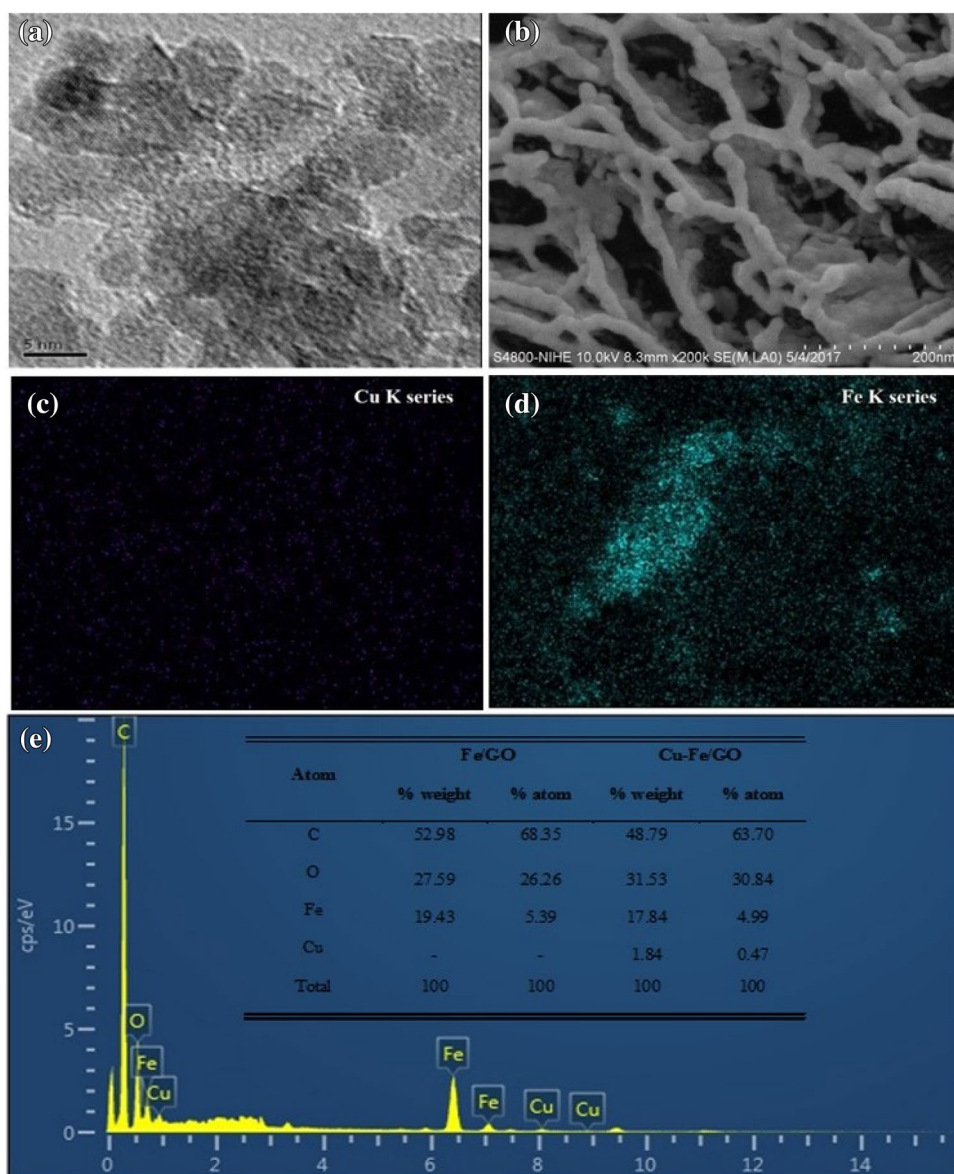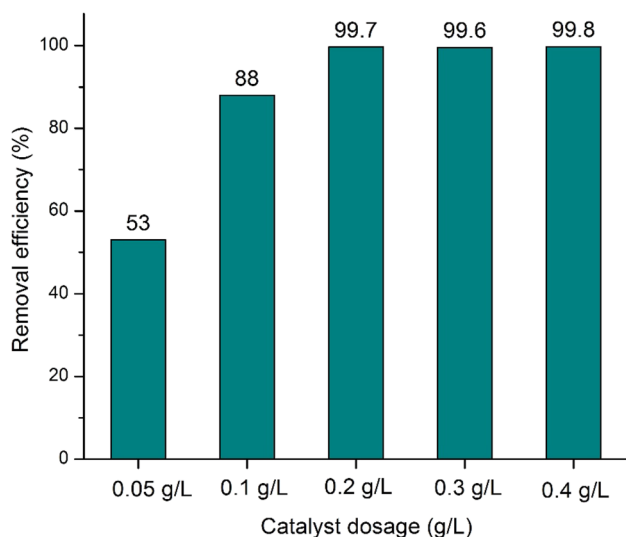**Fig. 4** **a** TEM image, **b** SEM image, **c**, **d** elemental mapping, **e** EDX spectrum of Cu–Fe/GO


**Fig. 5** **a** N_2 adsorption–desorption isotherms and **b** pore size distribution of GO and Cu–Fe/GO

Table 1 Textural properties of GO and Cu–Fe/GO nanocomposite

Sample	S_{BET}[a] (m^2 g^{-1})	V_{total}[b] (cm^3 g^{-1})	V_{micro}[c] (cm^3 g^{-1})	Pore size[d] (nm)
GO	331	1.719	0.002	20.7
Cu–Fe/GO	130	0.410	0.003	12.6

[a]Multipoint BET surface area

[b]total pore volume at $P/P_0 = 0.99$

[c]micropore volume by the t-plot method and

[d]average pore size by BET method (4 V/S.A)

Fig. 6 Effect of Cu–Fe/GO dosage for the photocatalytic degradation of DDT

$$OH \cdot + H_2O_2 \rightarrow OH_2 \cdot + H_2O \qquad (1)$$

$$OH_2 \cdot + OH_2 \cdot \rightarrow H_2O_2 + O_2 \qquad (2)$$
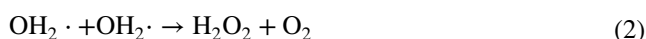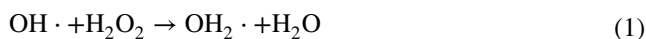
3.2.2 Degradation of DDT by Adsorption, Fenton Process and Photo-Fenton Process

After tuning the parameters, the optimal condition was used to study the degradation of DDT by adsorption, Fenton process and Photo-Fenton process using Cu–Fe/GO (Fig. 9a). The adsorption process has shown around 40% DDT removal efficiency for 3 h. Moreover, the Fenton process and Photo-Fenton process have shown DDT removal efficiency 85% and 99.2% respectively. High efficiency was obtained by the Photo-Fenton process compared with the Fenton process and adsorption process. It was attributed to the presence of Cu^+ ions (from XPS) which reduced Fe^{3+} to Fe^{2+} ion and provided more –OH radicals under visible
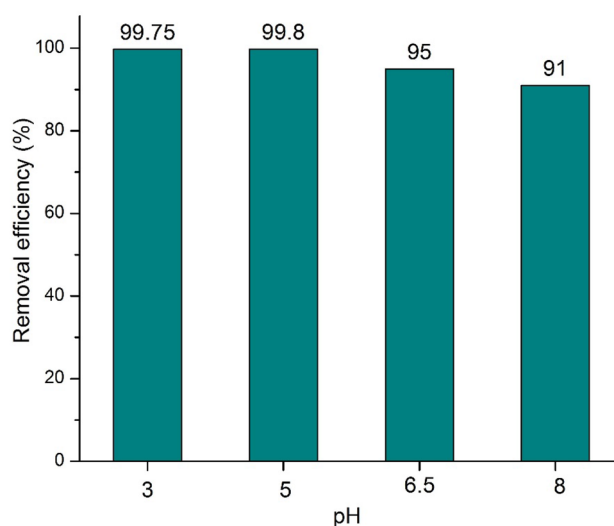
Fig. 7 Photocatalytic degradation of DDT at different pH of DDT solution using Cu–Fe/GO
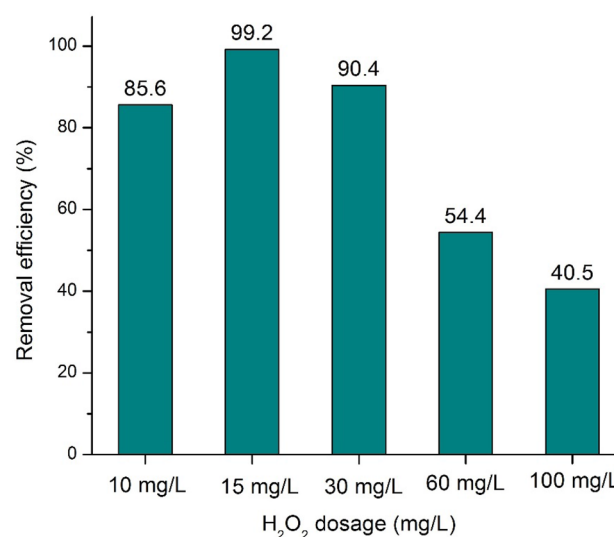
Fig. 8 Effect of H_2O_2 dosage for the photocatalytic degradation of DDT using Cu–Fe/GO

light irradiation [36, 39]. Figure 9b shows DDT removal efficiency using Fe/GO and Cu–Fe/GO catalysts by the Photo-Fenton process. Cu–Fe/GO has shown high DDT removal efficiency compared with Fe/GO by the promotional effect of copper.

Persistent organic pollutants degradation by advanced oxidation process using Photo-Fenton catalyst is one of the effective methods. Our results have shown that DDT was completely oxidized into CO_2, H_2O, and HCl. For better
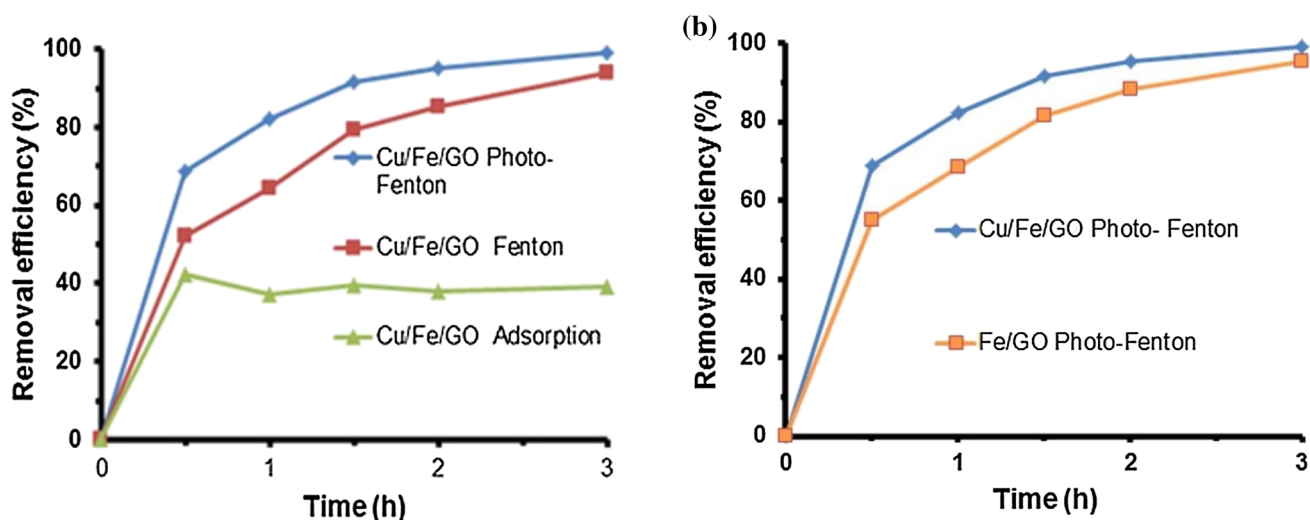
Fig. 9 DDT removal efficiency: **a** by adsorption, Fenton process and Photo-Fenton process using Cu–Fe/GO, **b** Photo-Fenton process using Fe/GO and Cu–Fe/GO

understanding, the reaction mechanism and intermediates produced during the reaction were analyzed by LC–MS. From the formed intermediates, the possible reaction pathway was: (i) dechlorination of DDT step by step, (ii) breaking of carbon chains and de-cyclization to form hydrocarbon with shorter chain, (iii) complete oxidation of hydrocarbon to form CO_2 and H_2O (Fig. 10). The shorter chain hydrocarbons (C_{14}, C_{12}, C_7 and C_6) identified in the DDT degradation process was good agreement with reported literature [40, 41].

3.3 Stability of Cu–Fe/GO Nanocomposite

Recyclability of the photocatalyst Cu–Fe/GO was studied up to 4 cycles (Fig. 11a). In each cycle, the catalyst was separated from the equilibrium solution by filtration then washed with methanol and dried at 60 °C overnight. In the 1st cycle, DDT removal efficiency was 99.2%. After 4 cycles, it was reached to 90.4%. The used catalyst was characterized by XRD (Fig. 11b). There was a change in the intensity of the peak at $2\theta = 24°$. It was due to the leaching of iron. However, no change in morphology has been observed (Fig. 11c). From these results, the synthesized Cu–Fe/GO nanocomposite catalyst has shown high photocatalytic degradation of DDT.

4 Conclusion

In this work, Fe/GO and Cu–Fe/GO nanocomposite were used for the photocatalytic degradation of dichlorodiphenyltrichloroethane in aqueous solution. Characterization results have confirmed that oxides of Cu and Fe were presented as
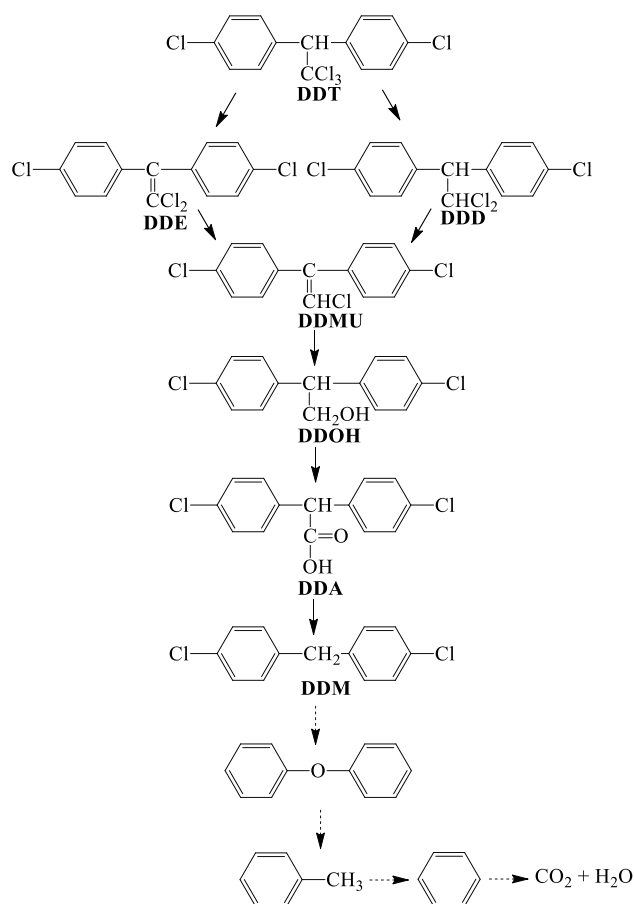

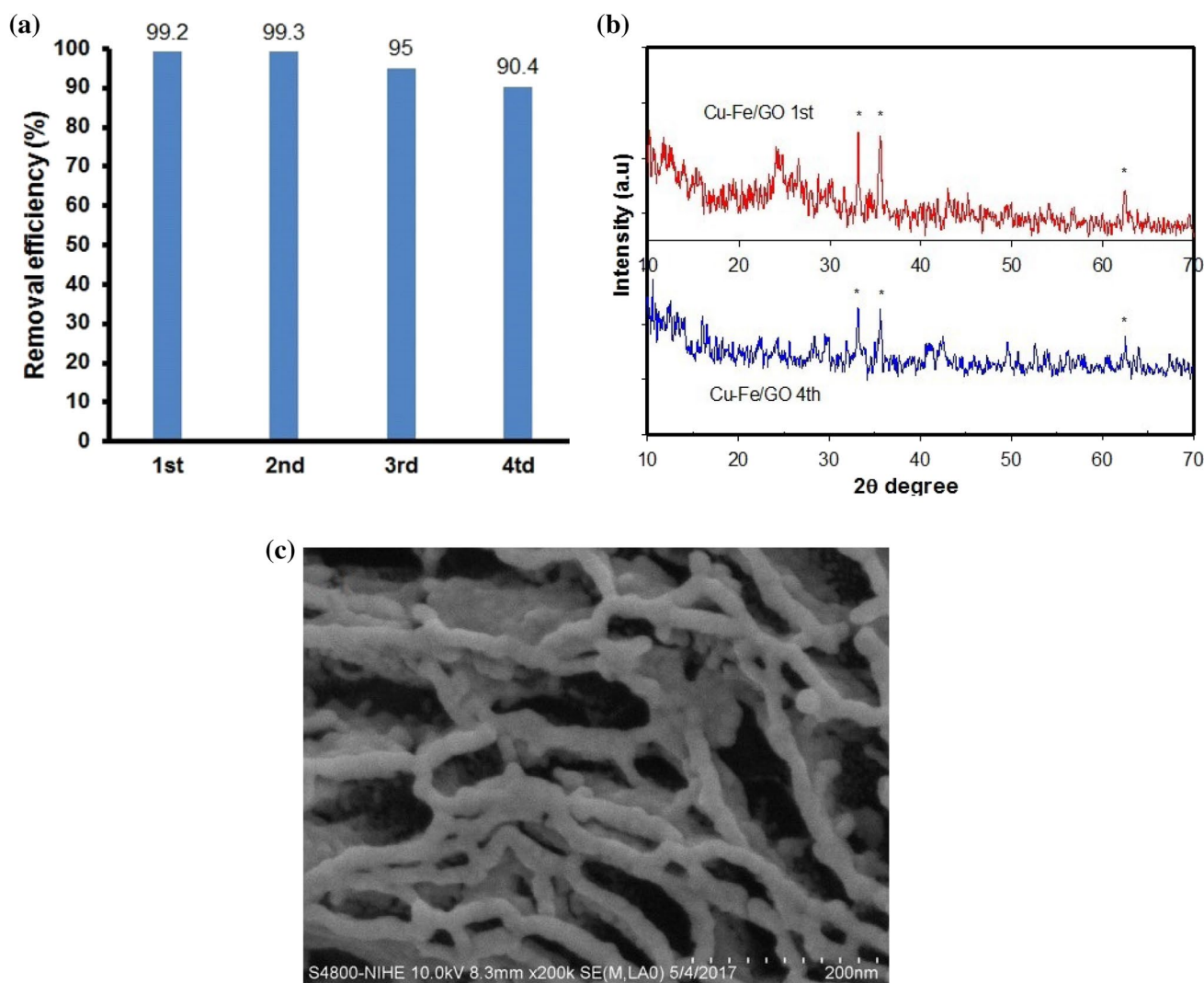**Fig. 10** Proposed DDT decomposition pathway using Cu–Fe/GO catalyst

Fig. 11 **a** Recyclability study, **b** XRD of fresh and used and **c** SEM image of Cu–Fe/GO

CuO and Fe_2O_3 on the graphene oxide. Cu–Fe/GO nanocomposite has obtained high DDT removal efficiency at pH of the DDT solution < 5 by the formation –OH radicals which enhanced DDT removal efficiency. Moreover, it has also shown high DDT removal efficiency compared with Fe/GO by the promotional effect of copper. In the recycle study, Cu–Fe/GO has shown good photocatalytic stability. Hence, graphene oxide supported metal oxides could be considered as an efficient and promising photocatalyst for the degradation of persistent organic pollutants.

References

1. Zhao M, Wang C, Zhang C, Wen Y, Liu W (2012) Enantioselective cytotoxicity profile of o, p′-DDT in PC 12 cells. PLoS ONE 7(8):e43823. https://doi.org/10.1371/journal.pone.0043823

2. Tian H, Li J, Zou L, Mu Z, Hao Z (2009) Removal of DDT from aqueous solutions using mesoporous silica materials. J Chem Technol Biotechnol 84(4):490–496. https://doi.org/10.1002/jctb.2067

3. Konstantinou IK, Albanis TA (2003) Photocatalytic transformation of pesticides in aqueous titanium dioxide suspensions using artificial and solar light: intermediates and degradation pathways. Appl Catal B 42(4):319–335. https://doi.org/10.1016/S0926-3373(02)00266-7

4. Kang S, Liu S, Wang H, Cai W (2016) Enhanced degradation performances of plate-like micro/nanostructured zero valent iron to DDT. J Hazard Mater 307:145–153. https://doi.org/10.1016/j.jhazmat.2015.12.063

5. El-Temsah YS, Sevcu A, Bobcikova K, Cernik M, Joner EJ (2016) DDT degradation efficiency and ecotoxicological effects of two types of nano-sized zero-valent iron (nZVI) in water and soil. Chemosphere 144:2221–2228. https://doi.org/10.1016/j.chemosphere.2015.10.122

6. Tian H, Li J, Mu Z, Li L, Hao Z (2009) Effect of pH on DDT degradation in aqueous solution using bimetallic Ni/Fe nanoparticles. Sep Purif Technol 66(1):84–89. https://doi.org/10.1016/j.seppur.2008.11.018

7. Cheng M, Zeng G, Huang D, Lai C, Xu P, Zhang C, Liu Y (2016) Hydroxyl radicals based advanced oxidation processes (AOPs) for remediation of soils contaminated with organic compounds: a review. Chem Eng J 284:582–598. https://doi.org/10.1016/j.cej.2015.09.001

8. Wang N, Zheng T, Zhang G, Wang P (2016) A review on Fenton-like processes for organic wastewater treatment. J Environ Chem Eng 4(1):762–787. https://doi.org/10.1016/j.jece.2015.12.016

9. Wang M, Fang G, Liu P, Zhou D, Ma C, Zhang D, Zhan J (2016) Fe_3O_4@β-CD nanocomposite as heterogeneous Fenton-like catalyst for enhanced degradation of 4-chlorophenol (4-CP). Appl Catal B 188:113–122. https://doi.org/10.1016/j.apcatb.2016.01.071

10. Cheng R, Li G-q, Cheng C, Shi L, Zheng X, Ma Z (2015) Catalytic oxidation of 4-chlorophenol with magnetic Fe_3O_4 nanoparticles: mechanisms and particle transformation. RSC Adv 5(82):66927–66933. https://doi.org/10.1039/C5RA10433E

11. Xu LJ, Wang JL (2013) Degradation of chlorophenols using a novel Fe^0/CeO_2 composite. Appl Catal B 142–143:396–405. https://doi.org/10.1016/j.apcatb.2013.05.065

12. Xu L, Wang J (2015) Degradation of 2,4,6-trichlorophenol using magnetic nanoscaled Fe_3O_4/CeO_2 composite as a heterogeneous Fenton-like catalyst. Sep Purif Technol 149:255–264. https://doi.org/10.1016/j.seppur.2015.05.011

13. Vu TA, Le GH, Dao CD, Dang LQ, Nguyen KT, Dang PT, Tran HTK, Duong QT, Nguyen TV, Lee GD (2014) Isomorphous substitution of Cr by Fe in MIL-101 framework and its application as a novel heterogeneous photo-Fenton catalyst for reactive dye degradation. RSC Adv 4(78):41185–41194. https://doi.org/10.1039/C4RA06522K

14. Ma J, Yang Q, Wen Y, Liu W (2017) Fe-g-C_3N_4/graphitized mesoporous carbon composite as an effective Fenton-like catalyst in a wide pH range. Appl Catal B 201:232–240. https://doi.org/10.1016/j.apcatb.2016.08.048

15. Guo S, Zhang G, Guo Y, Yu JC (2013) Graphene oxide–Fe_2O_3 hybrid material as highly efficient heterogeneous catalyst for degradation of organic contaminants. Carbon 60:437–444. https://doi.org/10.1016/j.carbon.2013.04.058

16. Hossain MN, Wen J, Chen A (2017) Unique copper and reduced graphene oxide nanocomposite toward the efficient electrochemical reduction of carbon dioxide. Sci Rep 7(1):3184. https://doi.org/10.1038/s41598-017-03601-3

17. Wu K, Jing C, Zhang J, Liu T, Yang S, Wang W (2019) Magnetic Fe_3O_4@CuO nanocomposite assembled on graphene oxide sheets for the enhanced removal of arsenic(III/V) from water. Appl Surf Sci 466:746–756. https://doi.org/10.1016/j.apsusc.2018.10.091

18. Le GH, Ngo QT, Nguyen TT, Nguyen QK, Quan TTT, Vu LD, Lee GD, Vu TA (2018) High catalytic activity of phenol photodegradation from aqueous solution with novel Fe–Fe_3O_4–GO nanocomposite. J Mater Eng Perform 27(8):4225–4234. https://doi.org/10.1007/s11665-018-3496-2

19. Guo S, Zhang G, Yu JC (2015) Enhanced photo-Fenton degradation of rhodamine B using graphene oxide–amorphous $FePO_4$ as effective and stable heterogeneous catalyst. J Colloid Interface Sci 448:460–466. https://doi.org/10.1016/j.jcis.2015.02.005

20. Khan M, Tahir MN, Adil SF, Khan HU, Siddiqui MRH, Al-warthan AA, Tremel W (2015) Graphene based metal and metal oxide nanocomposites: synthesis, properties and their applications. J Mater Chem A 3(37):18753–18808. https://doi.org/10.1039/C5TA02240A

21. Bhunia P, Kim G, Baik C, Lee H (2012) A strategically designed porous iron–iron oxide matrix on graphene for heavy metal adsorption. Chem Commun 48(79):9888–9890. https://doi.org/10.1039/C2CC35120J

22. Chen J, Yao B, Li C, Shi G (2013) An improved Hummers method for eco-friendly synthesis of graphene oxide. Carbon 64:225–229. https://doi.org/10.1016/j.carbon.2013.07.055

23. Hou H, Hu X, Liu X, Hu W, Meng R, Li L (2015) Sulfonated graphene oxide with improved ionic performances. Ionics 21(7):1919–1923. https://doi.org/10.1007/s11581-014-1355-1

24. Ning W-S, Wang T, Chen H, Yang X, Jin Y (2017) The effect of Fe_2O_3 crystal phases on CO_2 hydrogenation. PLoS ONE 12:e0182955. https://doi.org/10.1371/journal.pone.0182955

25. Melero JA, Calleja G, Martínez F, Molina R (2006) Nanocomposite of crystalline Fe_2O_3 and CuO particles and mesostructured SBA-15 silica as an active catalyst for wet peroxide oxidation processes. Catal Commun 7(7):478–483. https://doi.org/10.1016/j.catcom.2006.01.008

26. Huang X, Zhou X, Qian K, Zhao D, Liu Z, Yu C (2012) A magnetite nanocrystal/graphene composite as high performance anode for lithium-ion batteries. J Alloys Compd 514:76–80. https://doi.org/10.1016/j.jallcom.2011.10.087

27. Pham VH, Cuong TV, Hur SH, Oh E, Kim EJ, Shin EW, Chung JS (2011) Chemical functionalization of graphene sheets by solvothermal reduction of a graphene oxide suspension in N-methyl-2-pyrrolidone. J Mater Chem 21(10):3371–3377. https://doi.org/10.1039/C0JM02790A

28. Sarkar C, Dolui SK (2015) Synthesis of copper oxide/reduced graphene oxide nanocomposite and its enhanced catalytic activity towards reduction of 4-nitrophenol. RSC Adv 5(75):60763–60769. https://doi.org/10.1039/C5RA10551J

29. Singh P, Nath P, Arun RK, Mandal S, Chanda N (2016) Novel synthesis of a mixed Cu/CuO-reduced graphene oxide nanocomposite with enhanced peroxidase-like catalytic activity for easy detection of glutathione in solution and using a paper strip. RSC Adv 6(95):92729–92738. https://doi.org/10.1039/C6RA20882G

30. Lu J, Jiao X, Chen D, Li W (2009) Solvothermal synthesis and characterization of Fe_3O_4 and γ-Fe_2O_3 nanoplates. J Phys Chem C 113(10):4012–4017. https://doi.org/10.1021/jp810583e

31. He Y, del Valle A, Qian Y, Huang Y-F (2017) Near infrared light-mediated enhancement of reactive oxygen species generation through electron transfer from graphene oxide to iron hydroxide/oxide. Nanoscale 9(4):1559–1566. https://doi.org/10.1039/C6NR08784A

32. Di Castro V, Ciampi S (1995) XPS study of the growth and reactivity of Fe/MnO thin films. Surf Sci 331–333:294–299. https://doi.org/10.1016/0039-6028(95)00190-5

33. Brunauer S, Emmett PH, Teller E (1938) Adsorption of gases in multimolecular layers. J Am Chem Soc 60(2):309–319. https://doi.org/10.1021/ja01269a023

34. Chen Q, Wu P, Dang Z, Zhu N, Li P, Wu J, Wang X (2010) Iron pillared vermiculite as a heterogeneous photo-Fenton catalyst for photocatalytic degradation of azo dye reactive brilliant orange X-GN. Sep Purif Technol 71(3):315–323. https://doi.org/10.1016/j.seppur.2009.12.017

35. Gürkan R, Kartal-Temel N, Ayan F (2015) Photocatalytic TiO2-catalyzed degradation of bromophenol blue-mediated Mo(IV)-peroxo complexes in the presence of SDS. Desalin Water Treat. https://doi.org/10.13140/RG.2.1.5186.1844

36. Hu X-j, Liu Y-g, Zeng G-m, Wang H, You S-h, Hu X, Tan X-f, Chen A-w, Guo F-y (2015) Effects of inorganic electrolyte anions on enrichment of Cu(II) ions with aminated Fe_3O_4/graphene oxide: Cu(II) speciation prediction and surface charge measurement. Chemosphere 127:35–41. https://doi.org/10.1016/j.chemosphere.2015.01.013

37. Yazici E, Deveci H (2010). Factors affecting decomposition of hydrogen peroxide. https://doi.org/10.13140/RG.2.1.1530.0648

38. Sahel K, Elsellami L, Mirali I, Dappozze F, Bouhent M, Guillard C (2016) Hydrogen peroxide and photocatalysis. Appl Catal B 188:106–112. https://doi.org/10.1016/j.apcatb.2015.12.044

39. Zhang J, Zhang X, Wang Y (2016) Degradation of phenol by a heterogeneous photo-Fenton process using Fe/Cu/Al catalysts. RSC Adv 6(16):13168–13176. https://doi.org/10.1039/C5RA20897A

40. Wang H, Tian H, Hao Z (2012) Study of DDT and its derivatives DDD, DDE adsorption and degradation over Fe-SBA-15 at low temperature. J Environ Sci 24(3):536–540. https://doi.org/10.1016/S1001-0742(11)60800-0

41. Pan X, Lin D, Zheng Y, Zhang Q, Yin Y, Cai L, Fang H, Yu Y (2016) Biodegradation of DDT by *Stenotrophomonas* sp. DDT-1: aharacterization and genome functional analysis. Sci Rep 6(1):21332. https://doi.org/10.1038/srep21332